

# Double-mode radial–non-radial RR Lyrae stars. OGLE-IV photometry of two high cadence fields in the Galactic bulge.

H. Netzel<sup>1\*</sup>, R. Smolec<sup>2†</sup> and P. Moskalik<sup>2</sup>

<sup>1</sup>*Instytut Astronomiczny, Uniwersytet Wrocławski, ul. Kopernika 11, 51-622 Wrocław, Poland*

<sup>2</sup>*Nicolaus Copernicus Astronomical Centre, Polish Academy of Sciences, Bartycka 18, 00-716 Warszawa, Poland*

Accepted . Received ; in original form

## ABSTRACT

We analyse the OGLE-IV photometry of the first overtone and double-mode RR Lyrae stars (RRc/RRd) in the two fields towards the Galactic bulge observed with high cadence. In 27 per cent of RRc stars we find additional non-radial mode, with characteristic period ratio,  $P_x/P_{1O} \in (0.6, 0.64)$ . It strongly corroborates the conclusion arising from the analysis of space photometry of RRc stars, that this form of pulsation must be common. In the Petersen diagram the stars form three sequences. In 20 stars we find two or three close secondary modes simultaneously. The additional modes are clearly non-stationary. Their amplitude and/or phase vary in time. As a result, the patterns observed in the frequency spectra of these stars may be very complex. In some stars the additional modes split into doublets, triplets or appear as a more complex bands of increased power. Subharmonics of additional modes are detected in 20 per cent of stars. They also display a complex structure.

Including our previous study of the OGLE-III Galactic bulge data, we have discovered 260 RRc and 2 RRd stars with the additional non-radial mode, which is the largest sample of these stars so far. The additional mode is also detected in two Blazhko RRc stars, which shows that the modulation and additional non-radial mode are not exclusive.

**Key words:** stars: horizontal branch – stars: oscillations – stars: variables: RR Lyrae

## 1 INTRODUCTION

RR Lyrae stars are considered to be textbook examples of simple, classical, radially pulsating variables. Indeed, majority of these stars pulsate in the fundamental mode (F mode, RRab stars) or in the first radial overtone (1O mode, RRc). A less frequent is simultaneous pulsation in these two radial modes (F+1O, RRd stars). Till very recently, a still mysterious quasi-periodic modulation of the pulsation amplitude and/or phase – the Blazhko effect (for a review see e.g. Szabó 2014) – was the only flaw in this simple picture.

With the advent of space based photometry and overwhelming amount of data gathered by ground-based photometric surveys, in particular by the Optical Gravitational Lensing Experiment (OGLE, Udalski et al. 2008; Udalski, Szymański & Szymański 2015), as well as by the dedicated ground based campaigns (e.g. Jurcsik et al. 2009),

the simple picture outlined above does not hold. Several stars pulsating simultaneously in the fundamental and in the second overtone were detected (for a review see Moskalik 2013). Many interesting discoveries in Blazhko variables were made, including discovery of period doubling in modulated RRab stars (Kolenberg et al. 2010; Szabó et al. 2010) or discovery of the Blazhko effect in RRd variables (Soszyński et al. 2014; Smolec et al. 2015; Jurcsik et al. 2014).

The most intriguing discovery however, seems to be the detection of non-radial modes in RRc stars, likely a common feature of these stars. The period of additional mode,  $P_x$ , is shorter than first overtone period; the period ratios,  $P_x/P_{1O}$ , fall in a narrow range between 0.60 and 0.64. The first detection of non-radial mode of this type was made in RRd star AQ Leo observed with the *MOST* satellite (Gruberbauer et al. 2007). Then, the same additional mode was also detected in 6 RRc stars in the globular cluster omega Centauri (Olech & Moskalik 2009). Other RRc stars with similar period ratios were discovered in the

\* E-mail: henia@netzel.pl

† E-mail: smolec@camk.edu.pl

OGLE LMC data (Soszyński et al. 2009) and in the SDSS data (Süveges et al. 2012). A big surprise was the analysis of 4 RRc stars observed with *Kepler* space telescope (Moskalik et al. 2015). In all these stars additional mode with characteristic period ratio in a range  $\sim (0.61, 0.63)$  was detected. Analysis of the *CoRoT* photometry (Szabó et al. 2014) and *K2*<sup>1</sup> observations (Molnár et al. 2015) leave no doubt: in 13 out of 14 RRc stars observed from space the additional mode is detected<sup>2</sup> – the phenomenon must be common in RRc stars.

Possible existence of a new group of double-periodic pulsators with period ratio close to 0.61 was postulated already by Olech & Moskalik (2009) and fully confirmed with the analysis of the *Kepler* photometry (Moskalik et al. 2013, 2015). In all these stars first overtone pulsation is dominant. The additional mode may also occur in RRd variables. Sub-harmonics of the additional mode are detected in the majority of stars observed from space and seem characteristic for this group. In the following we will refer to these stars as 0.61-stars. The period ratio, cannot correspond to two radial modes, as model computations clearly show – it is in between period ratios expected for 1O+3O and 1O+4O pulsators (Moskalik et al. 2015).

The additional mode in 0.61-stars is of low amplitude, in the mmag range, typically, 1 to 4 per cent of the first overtone amplitude. The low amplitude makes the detection of additional mode difficult from the ground. Nevertheless, in our analysis of the OGLE-III photometry of the Galactic bulge (Netzel, Smolec & Moskalik 2015), we have found 147 RRc and RRd stars with the additional mode (3 per cent of OGLE-III RRc sample), increasing the number of known stars of this type by factor 6 and allowing first statistical analyses. In the Petersen diagram majority of these stars form a tight sequence with period ratios clustering around 0.613. A signature of a second sequence with slightly larger period ratio (0.63) was also detected.

Here we report the analysis of the top-quality OGLE-IV data for the Galactic bulge RRc stars. A detection of 131 stars, which is 27 per cent of the analysed sample, together with recent results of Jurcsik et al. (2015), who report the detection of eighteen 0.61 stars in M3 ( $\sim 38$  per cent of their sample), corroborate the results of space mission – the phenomenon must be common among RRc stars. Our new results allow much more detailed analysis of the group. In several stars we detect very rich structures in the frequency spectrum. At the frequency range characteristic for the additional mode we observe one, two or even three well separated peaks; corresponding period ratios are in a range  $\sim (0.61 - 0.63)$ . These peaks give rise to three sequences in the Petersen diagram – in addition to two sequences we detected before, a third, although scarcely populated, clearly appears in between. Rich and complex structures are de-

<sup>1</sup> *K2* is the continuation of *Kepler* space telescope mission, with observations carried along ecliptic plane, after the second reaction wheel failure.

<sup>2</sup> The only RRc star observed from space in which additional mode is not detected shows the Blazhko effect. Still, only 8.9d of observations are available for this star and hence the presence of additional 0.61 mode cannot be excluded, specially taking into account its variable nature, see Section 3.2.

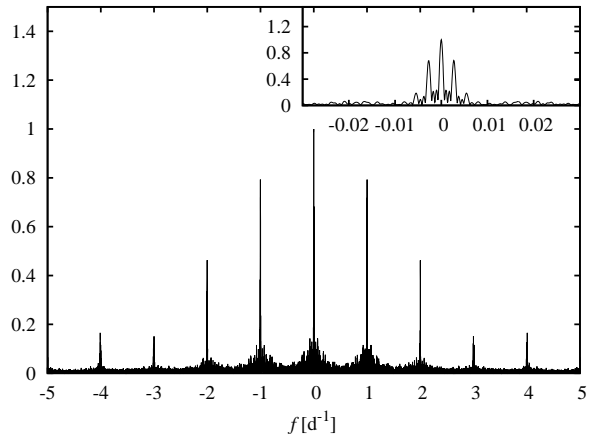


**Figure 1.** Example of spectral window for OGLE-IV data.

tected at frequency range around sub-harmonic of the additional mode(s).

## 2 DATA AND ANALYSIS

In the analysis we used data from the fourth phase of the OGLE project (Soszyński et al. 2014; Udalski, Szymański & Szymański 2015). In publicly available OGLE-IV data<sup>3</sup> there are four observational seasons covering 1334 days for most stars. OGLE-IV collection of variable stars contains 38 257 RR Lyrae stars from the Galactic bulge, including 10 825 RRc stars and 174 RRd stars. For the analysis we selected stars pulsating in the first overtone (RRc and RRd) placed in the most frequently observed fields (501 and 505 in OGLE-IV). This choice is motivated by our goal, search for low amplitude signals, which requires possibly the lowest noise level. This is met by stars with most numerous observations. There are more than 8 000 data points for each star. Selected sample consist of 485 RRc and 4 RRd stars. We used only *I*-band data, as they are much more numerous than *V*-band data. Spectral window for OGLE-IV data is presented in Fig. 1. It is typical for the OGLE photometry of the Galactic bulge. Strong 1-day and 1-year aliases are present.

All data were analysed manually. In the analysis we used standard successive prewhitening method. Significant frequencies were found with discrete Fourier transform and fitted to the data in the form:

$$m(t) = m_0 + \sum_{k=1}^N A_k \sin(2\pi f_k t + \phi_k), \quad (1)$$

where  $f_k$  are frequencies,  $A_k$  and  $\phi_k$  are amplitudes and phases. We considered only frequencies with signal-to-noise ratio  $S/N \geq 4$ . Then we performed detrending and data clipping with  $4\sigma$  criterion, where  $\sigma$  is the dispersion of the fit.

Slow trends are present in the data of many stars. In the frequency spectrum they produce signal at low frequencies which gives rise to daily aliases at around integer fre-

<sup>3</sup> <ftp://ftp.astrow.edu.pl/ogle/ogle4>

quency values. We modelled these trends with long-period sine function (50 000 d) or we removed them from the data with low-order polynomial.

In many stars, after prewhitening with the frequency of the first overtone,  $f_{10}$ , signals in the vicinity of  $f_{10}$  remain. They form either doublets of equidistant triplets and multiplets at the main frequency and its harmonics. These are manifestations of the Blazhko effect in the frequency spectrum. We fitted these signals in the form  $kf_{10} \pm n\Delta f$ , where  $\Delta f$  is a separation between main frequency and the side peaks.

In some stars signals at the location of  $f_{10}$  or its harmonics remained despite prewhitening. It is caused by the change of amplitude and/or phase of the first overtone on time-scale longer than data length. Non-stationary signals result in higher noise level, give raise to daily aliases, and so hamper the search for additional low amplitude signals. In order to remove such signals we used time-dependent prewhitening method proposed by Moskalik et al. (2015). Its application to OGLE data is described in more detail in Netzel, Smolec & Moskalik (2015). In cases of stars for which OGLE-III data (Soszyński et al. 2011) are available we merged the data in order to investigate long-term changes of the first overtone. Irregular phase variations are frequent, but in some cases analysis of the merged data revealed long-period Blazhko effect.

For all stars for which we found additional periodicity of interest,  $f_x$ , we conducted seasonal analysis. Analysis, as described above, was performed on each of the four observing seasons separately in order to investigate time variation of the additional periodicity (Section 3.2).

In this paper our attention is focused only on 0.61-stars. In the same sample of stars we have detected yet another intriguing group of double-periodic radial-non-radial variables, with period of the additional mode longer than first overtone period. This result was reported in Netzel, Smolec & Dziembowski (2015). Detailed analysis of the Blazhko effect in RRc stars is in preparation.

### 3 RESULTS

#### 3.1 Overview

We have found 131 RRc stars with the additional non-radial mode of interest (27 per cent of the analysed sample). Period ratios with the first overtone period,  $P_x/P_{10}$ , fall in a range  $\sim (0.60, 0.64)$ . Out of four analysed RRd stars none shows the additional mode. 16 stars from the present sample were already discovered in our previous analysis of the OGLE-III data (Netzel, Smolec & Moskalik 2015). Altogether, our analysis of the OGLE Galactic bulge data led to the discovery of 262 stars of this type, to be compared with only 23 previously known (summarised in Moskalik et al. 2015) and 18 discovered recently by Jurcsik et al. (2015).

Basic properties of all stars are collected in Tab. A1 in the Appendix, sample of which is shown in Tab. 1. Subsequent columns contain period of the first overtone and of the additional mode(s), their ratio, amplitude of the first overtone,  $A_{10}$ , amplitude of the additional mode(s),  $A_x$ , and amplitude ratio,  $A_x/A_{10}$ . Remarks are given in the last column. For some stars there are more than one line in the

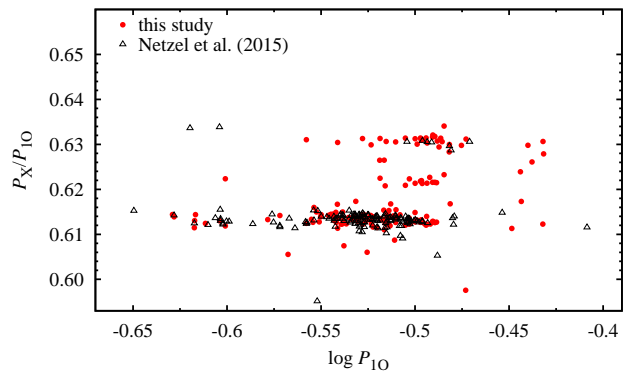


**Figure 2.** Petersen diagram for 0.61 stars from OGLE-IV sample analysed in this paper (red filled circles) and OGLE-III sample from our previous study (triangles; Netzel, Smolec & Moskalik 2015).

table. For these stars we detect two or three significant, well separated frequencies in the frequency range of interest, i.e.  $f/f_{10} \in (0.60, 0.64)^{-1}$ . Criterion for selecting the frequencies entering the table is described in the following paragraphs.

Data from Tab. A1 are plotted in the Petersen diagram in Fig. 2 together with the results of our study of OGLE-III Galactic bulge data (Netzel, Smolec & Moskalik 2015). For 20 stars more than one point appears in the diagram (stars with more than one line in Tab. A1).

In case of many stars there are many resolved peaks with  $S/N \geq 4$  in the frequency range of interest. Examples are presented in Fig. 3. Note that in this and other figures presenting frequency spectra, we use a more convenient, normalized period scale for horizontal axis, i.e. we plot frequency spectra vs.  $P/P_{10} = f_{10}/f$ . This allows a direct comparison with the Petersen diagram. Usually the signals appear as a relatively narrow cluster of peaks centered at a characteristic frequency. Panel a of Fig. 3 shows OGLE-BLG-RRLYR-04754, which displays such cluster of peaks centered at  $P/P_{10} \approx 0.613$ . Next two panels show analogous clusters of peaks, but centered around 0.622 (panel b) and 0.631 (panel c). In case of these and similar stars only the frequency and amplitude of the highest peak in a cluster is included in Tab. A1, regardless whether other signals from the cluster have  $S/N \geq 4$  (before or after prewhitening). Those stars are marked with ‘g’ in the remarks column of Tab. A1.

Such structures, with signals in three different, rather characteristic locations, are most commonly found in the frequency spectra of the analysed stars. As a result three sequences in the Petersen diagram emerge (Fig. 2). Most of the stars are placed in the lowest sequence. It is horizontal and centered at  $P_x/P_{10} \approx 0.613$  value. It also covers the largest range of periods. Less populated sequence is the highest one. It is centered at  $P_x/P_{10} \approx 0.631$ . A slight trend of decreasing period ratio with increasing period of the first overtone is visible in this sequence. A third sequence is weakly populated but well visible in Fig. 2, in between the two previously described sequences. It appears horizontal, is centered at  $P_x/P_{10} \approx 0.623$  and covers mostly a small range of periods around  $\log P_{10} = -0.5$ . Although stars which fit this sequence were also detected in previous stud-

**Table 1.** Sample table with properties of stars with non-radial mode (OGLE-IV). Full Table is in the Appendix.

Name	$P_{1O}$ [d]	$P_x$ [d]	$P_x/P_{1O}$	$A_{1O}$ [mag]	$A_x$ [mag]	$A_x/A_{1O}$	Remarks
OGLE-BLG-RRLYR-04067	0.31994	0.19592	0.61236	0.10687	0.00479	0.0448	a
OGLE-BLG-RRLYR-04105	0.30582	0.18724	0.61226	0.13009	0.00476	0.0366	
OGLE-BLG-RRLYR-04549	0.29964	0.18874	0.62990	0.12246	0.00384	0.0313	
OGLE-BLG-RRLYR-04599	0.28939	0.17797	0.61498	0.13980	0.00340	0.0243	a,g
OGLE-BLG-RRLYR-04754	0.28631	0.17578	0.61394	0.12788	0.00453	0.0354	g,h
OGLE-BLG-RRLYR-04762	0.29465	0.18061	0.61295	0.12640	0.00700	0.0554	
...							

ies (4 stars in Jurcsik et al. (2015) and 4 stars from tab. 8 in Moskalik et al. (2015)), the fact, that they form a third sequence became evident only in the OGLE-IV data. The three sequences are almost equidistant in the Petersen diagram. A significant spread of period ratios is present within each sequence. It is a consequence of the just described form in which signals appear in the frequency spectrum. The signals in a cluster of peaks are of almost equal height (Fig. 3). Which peak is the highest and hence included in Tab. A1/ Fig. 2 is a matter of chance, taking into account the relatively small  $S/N$  for these peaks, typically around 5 – 6.

Although this choice is, out of necessity, a bit arbitrary, based on Fig. 2 and using data only for the stars detected in homogeneous OGLE Galactic bulge samples, we can estimate the values of period ratio separating the three sequences. These fall around  $P_x/P_{1O} \approx 0.620$  and  $P_x/P_{1O} \approx 0.628$ . The three sequences selected this way are named 0.61-, 0.62- and 0.63-sequences in the following.

In several stars, the clusters of peaks seem to form triplets. These stars are marked with ‘t’ in the remarks column of Tab. A1. Panel d in Fig. 3 shows an example of such triplet visible in a spectrum of OGLE-BLG-RRLYR-05600, which belongs to 0.61 sequence. The highest peak is detected in the central component of the triplet and its frequency/amplitude are included in Tab. A1. It may also happen that the highest peak in the triplet is detected in its side component. This is the case for OGLE-BLG-RRLYR-04974 (panel e in Fig. 3), another star from 0.61 sequence. Its frequency is then reported in Tab. A1/ Fig. 2. The spread of period ratios within 0.61 sequence (Fig. 2) is partially due to the appearance of such triplets with various heights of the triplet components. We also note that the separation between the triplet components (their midpoints) is approximately equal (see also Sect. 3.5 and 4). In a few stars we observe doublets instead of triplets. These stars are marked with ‘d’ in the remarks column of Tab. A1. We note that triplets and doublets appear preferentially in the lowest, 0.61 sequence, and only rarely in the two others.

Besides single clusters of peaks (panels a, b and c in Fig. 3), and multiplet-like structures (panels d and e), there are more complex structures which are not easily classifiable (‘f’ in remarks column). Two examples are presented in panels f and g in Fig. 3: OGLE-BLG-RRLYR-09164 and OGLE-BLG-RRLYR-08824. In case of the first star, there is a power excess covering a rather wide frequency range. The second star has several signals between 0.61 and 0.62, which do not form a triplet-like structure. In all those stars the highest peak is chosen for the table and the Petersen

diagram. The complex structures appear only in the lowest, 0.61 sequence.

To get more insight into appearance of the discussed complex structures in the frequency spectra, in Fig. 4 we present a comparison between spectral window and  $f_x$  signal in two stars. Middle panel of this figure shows spectrum of OGLE-BLG-RRLYR-07907 centered at  $f_x$ . In this star additional signal is discrete and can be subtracted from the data with a single sine function. Structure is similar to the spectral window shown on the bottom panel. Upper panel in Fig. 4 shows the additional mode in OGLE-BLG-RRLYR-04754 (this star is also shown in panel ‘a’ of Fig. 3 in wider frequency range). The mode appears as a cluster of peaks rather than a single and coherent peak.

Similar structures to described above were also detected in the *Kepler* RRc data (e.g. Fig. 12 in Moskalik et al. 2015, see also Section 3.5).

Some stars are important exceptions from the scenario outlined above and detected in space observations of RRc stars. In Fig. 5 we present frequency spectra for six stars in which we observe simultaneously three signals falling into three sequences defined above. Again, typically, we do not observe three single peaks, but three clusters of peaks centered at frequencies characteristic for the three sequences. For these stars, data for the highest peak in each of the three clusters are given in Tab. A1 (three rows) and in the Petersen diagram (Fig. 2) each of these stars is represented by three points. We also find stars with two clusters of peaks corresponding to two of the three sequences we defined. Examples are shown in Fig. 6. For these stars, data for two highest peaks, one from each cluster, are given in Tab. A1 and two points are plotted in the Petersen diagram.

We also note that in several stars in which only one additional peak belonging to one of the sequences is present, we observe a power excess centered at frequency characteristic for other sequences. Since these bumps of power excess are below  $S/N$  of 4 no additional information is included in Tab. A1 and such stars are represented in the Petersen diagram with only one point.

Amplitudes of the additional modes are very low compared to amplitudes of the first overtone mode. Histogram of amplitude ratio,  $A_x/A_{1O}$ , for all analysed stars is shown in Fig. 7. Amplitudes of the additional modes vary from 0.6 per cent to 5.5 per cent of the first overtone amplitude with average value of 2 per cent.

In Fig. 8 we present the color-magnitude diagram for RRc stars in the two analysed OGLE-IV fields. Stars with the additional mode follow a progression of single-periodic RRc stars and are not restricted to any particular color

range in the diagram. We note however, that the large extent of the progression is caused by the different reddenings towards the observed stars, which is characteristic for the extended Galactic bulge population.

In Fig. 9 we show the histogram of first overtone period distribution for RRc stars in the two analysed fields. The 0.61 stars are not confined to any particular period range. The distribution peaks in between 0.28 and 0.32 d, but both long and short period 0.61 stars are also present. Together with the color-magnitude plot, it suggests that 0.61 stars are not confined to any particular part of the HR diagram, but are distributed over entire first overtone instability strip (cf. with Jurcsik et al. 2015).

16 stars, which were discovered earlier in OGLE-III data (Netzel, Smolec & Moskalik 2015), are marked in Tab. A1 with ‘h’ in remarks. There is no significant difference between properties of these stars determined from OGLE-III and from OGLE-IV data. For a few stars, in OGLE-IV data we detected subharmonics and combination frequencies of the first-overtone and of the additional mode, which were undetected in OGLE-III data. In three stars we detected frequencies belonging to more than one of the three sequences described earlier. Due to high observing cadence, the noise level in OGLE-IV data is much lower, which makes detection of other, low-amplitude signals possible.

### 3.2 Seasonal variations

Complex structures observed in the frequency spectrum at the frequencies of the additional modes and at their vicinity indicate strong non-stationarity of the modes. In order to investigate the variation of the additional signals, we analysed separately each of the four observing seasons. Example of seasonal analysis is shown in Fig. 10 for OGLE-BLG-RRLYR-07806. First four panels correspond to subsequent observing seasons. Last panel shows the frequency spectrum of all data analysed together. The green dotted line indicates  $S/N = 4$ . Analysis of the whole dataset shows three clusters of signals corresponding to the three sequences on the Petersen diagram, with  $P_x/P_{10} \sim 0.61$ ,  $\sim 0.62$  and  $\sim 0.63$ .

Analysis of each season separately shows strong variability within each cluster. In the first observing season, peaks from the two sequences, 0.61 and 0.62, are significant. In the second observing season we clearly detect three peaks, each corresponding to one of the sequences. Signal corresponding to 0.63 sequence is the highest. In the third observing season there is only one signal from 0.62 sequence. Analysis of the fourth observing season does not reveal any significant frequencies in the range of interest, however power excess is obvious at the expected locations. Amplitudes and frequencies of the observed signals clearly vary, producing, in the frequency spectrum of all data, three clusters of peaks, rather than three coherent peaks.

Seasonal changes described above are characteristic for most stars. Frequency and amplitude of the additional mode vary from season to season in every star. Changes are irregular (for an example see also fig. 9 in Netzel, Smolec & Moskalik 2015). Also, signals corresponding to different sequences vary differently, which is well visible in Fig. 10.

We note that the OGLE data do not allow more detailed analysis than on a season-to-season basis. On the

other hand, we know, at least from *Kepler* observations of this type of stars (Moskalik et al. 2015), and the appearance of the frequency spectra, that the variation may occur on a much shorter time scale, which is averaged out in our analysis.

Seasonal analysis discussed above indicates that the additional non-radial modes could be excited in other RRc stars of our sample, not listed in Tab. A1. One can imagine that the signals are strong only during one or two seasons, but in the analysis of the whole dataset they just manifest as power excess at expected frequencies, but below the adopted detection threshold ( $S/N = 4$ ). This is indeed the case. In some stars, presented in Fig. 6, with significant signals belonging to two of the three sequences, a power excess at the location expected for the remaining, third sequence, is also present, but is too low to be considered significant. Consequently it was not included in the Tab. A1.

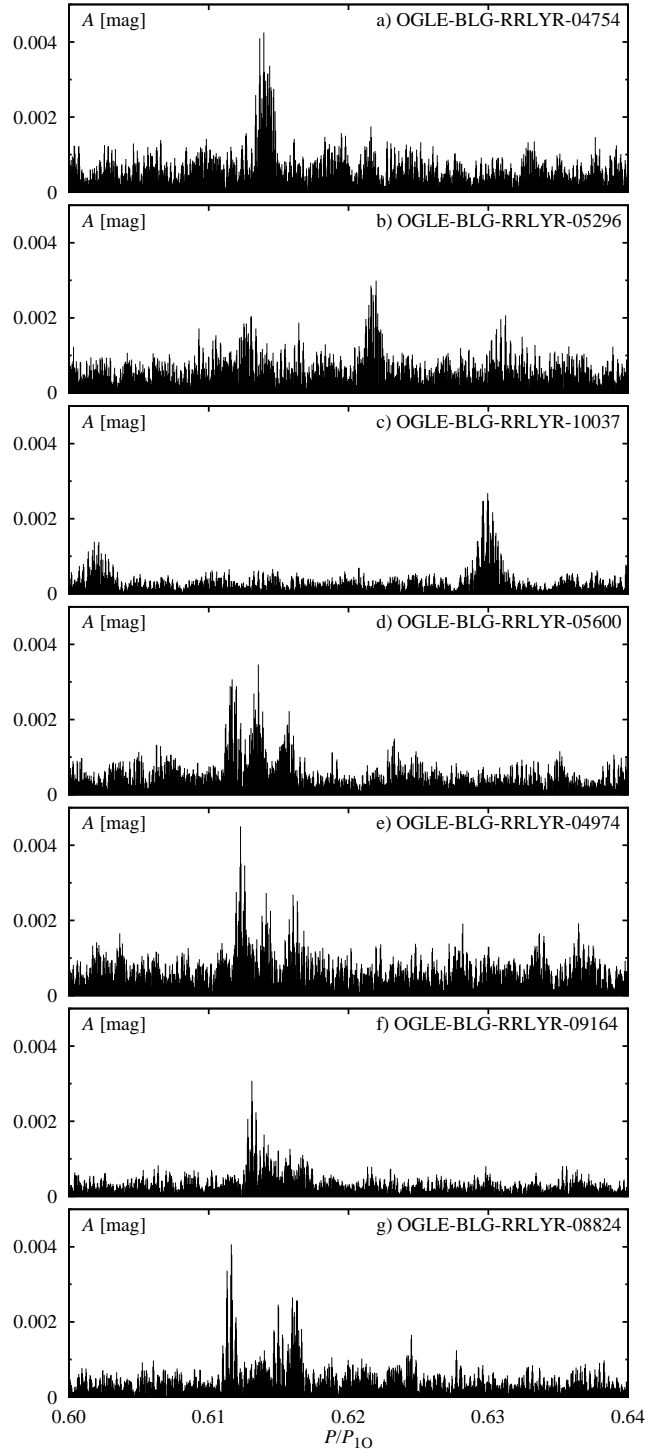


**Figure 3.** Examples of signal structures detected in the frequency spectra of 6 stars at frequency range characteristic for additional modes discussed in this paper. Note, that horizontal axis is a normalized period scale, ie.,  $P/P_{10} = f_{10}/f$ .

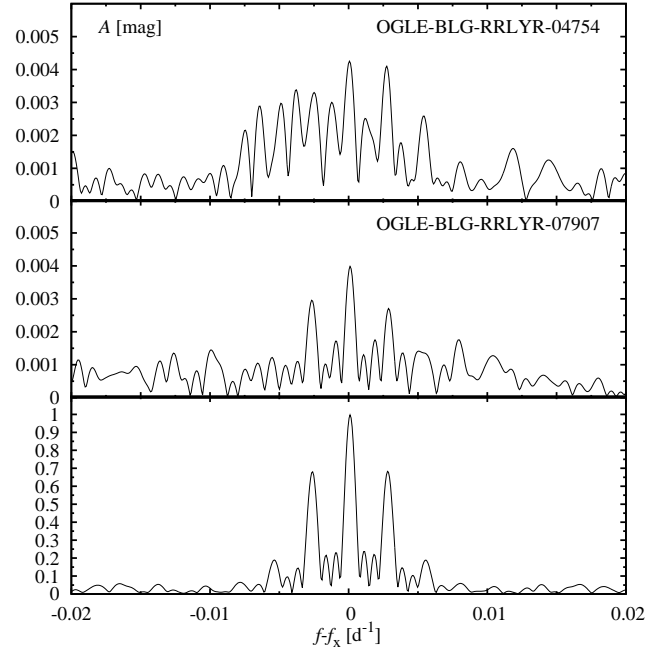


**Figure 4.** Comparison of signal at  $f_x$  for two stars (two upper panels) with spectral window (bottom panel).

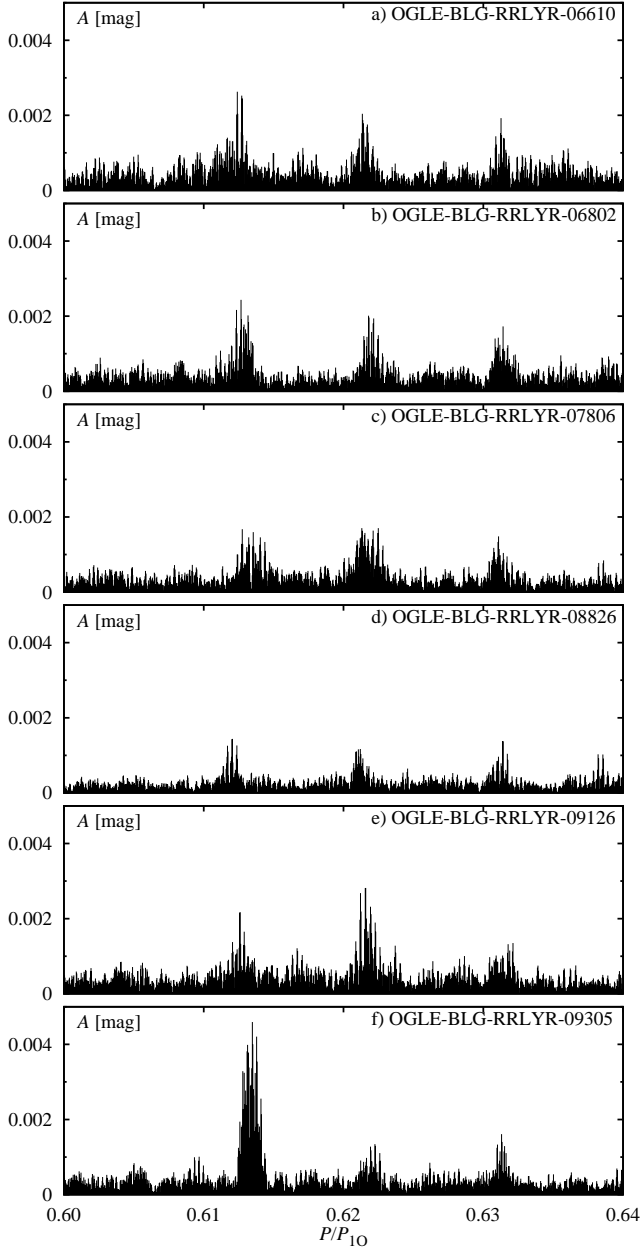


**Figure 5.** Frequency spectra for 6 stars in which we detect significant peaks corresponding to three different sequences in the Petersen diagram, Fig. 2.

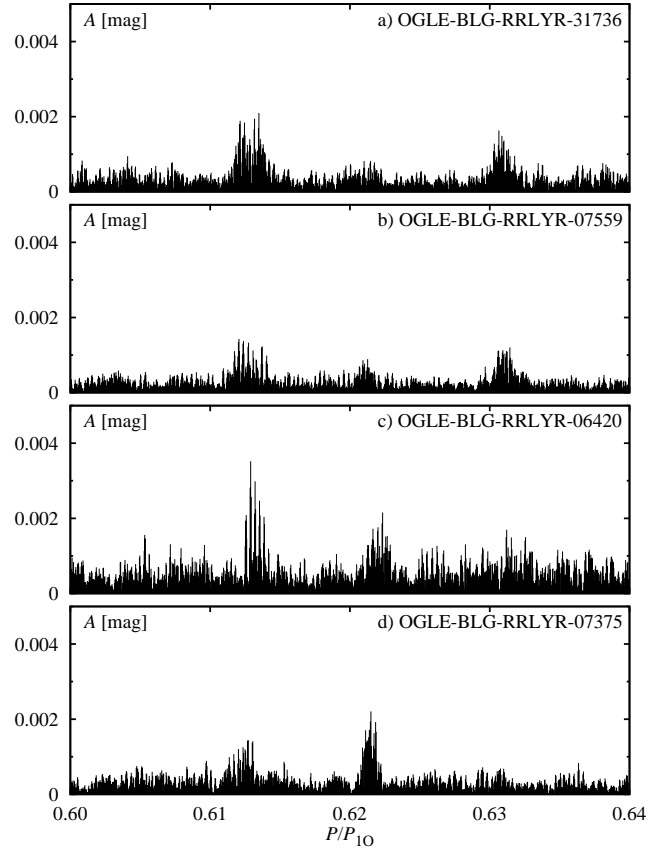


**Figure 6.** Frequency spectra for stars in which we detect significant signals corresponding to two of the three sequences in the Petersen diagram, Fig. 2.

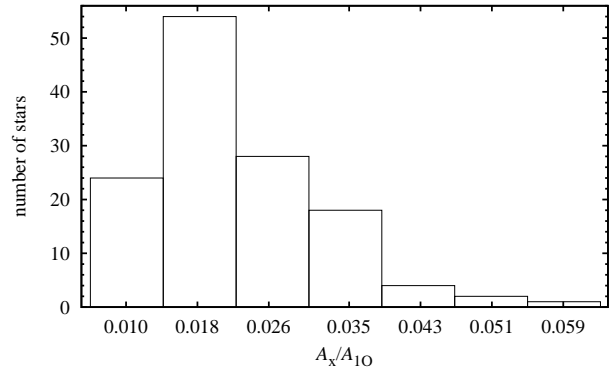


**Figure 7.** Histogram of amplitude ratios,  $A_x/A_{10}$ . One signal for each star included.

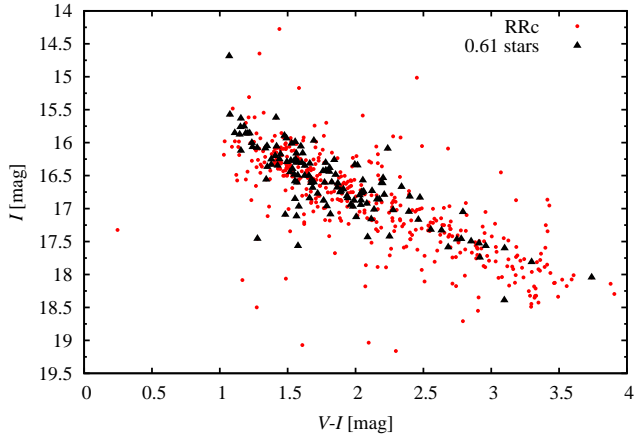


**Figure 8.** The observed color-magnitude diagram for RRc stars in the two analysed OGLE-IV fields.

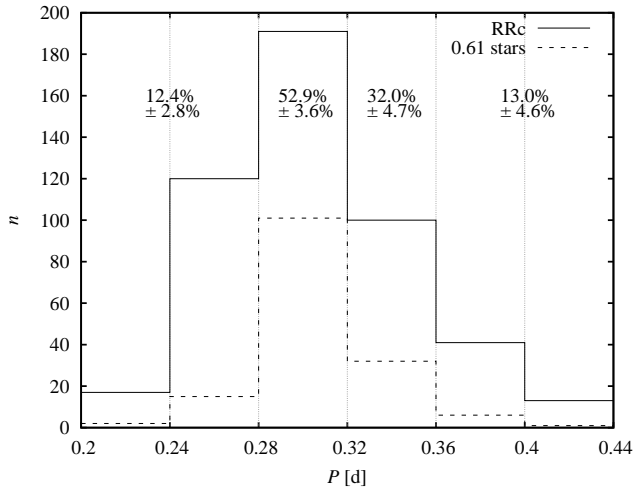


**Figure 9.** Histogram of periods,  $P_{IO}$ , for RRc sample and 0.61 stars. Incidence rate for 0.61 stars is calculated in four bins. Outer bins are merged, because of a small number of stars. Statistical errors of the incidence rates were calculated assuming that the population follows a Poisson distribution (e.g. Alcock et al. 2003).

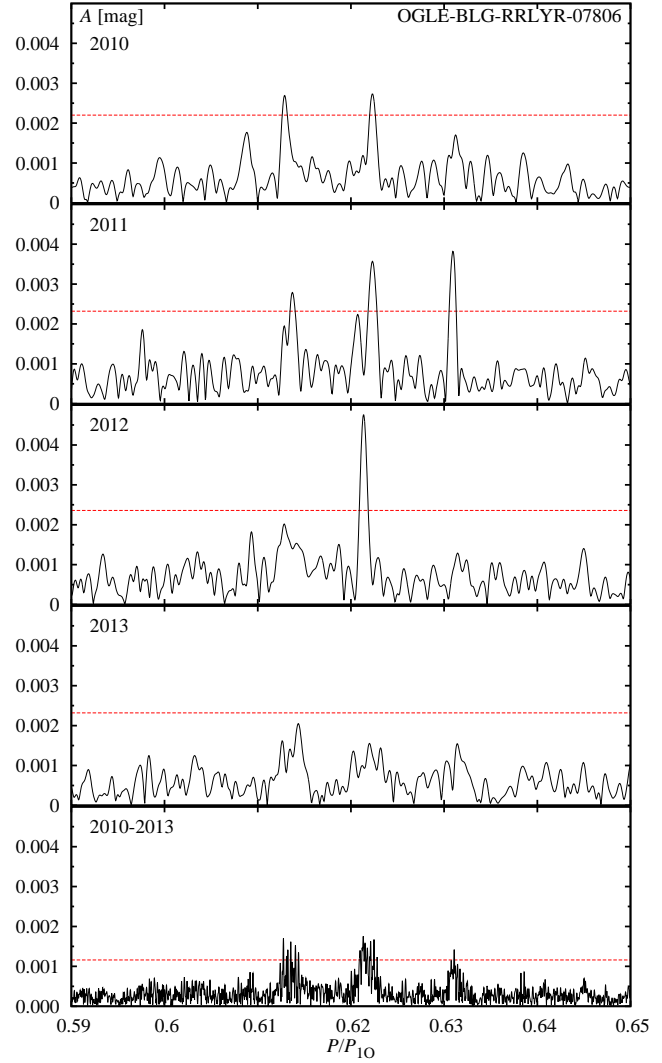


**Figure 10.** Frequency spectra for each of the four observation seasons (first four panels) for OGLE-BLG-RRLYR-07806 at the frequency range of interest. Last panel shows frequency spectrum of all the data. Horizontal line indicates the  $4\sigma$  noise level.



### 3.3 Subharmonic frequency range

Significant signals at subharmonics of the additional mode are commonly detected in RRc stars observed from space, both at  $1/2f_x$  and at  $3/2f_x$  (Szabó et al. 2014; Moskalik et al. 2015; Molnár et al. 2015). In the ground based observations subharmonics are hard to detect. Only in Netzel, Smolec & Moskalik (2015) we reported a weak signals at  $1/2f_x$  in four stars.

In OGLE-IV data we detect significant signals at around subharmonic of additional mode(s), i.e. at around  $1/2f_x$ , in 26 stars. These stars are marked with ‘s’ in the remarks column of Tab. A1. Only in two stars we detect signal at around  $3/2f_x$  with  $S/N > 4$ . Strictly, we do not detect single peaks exactly at  $1/2f_x$  or at  $3/2f_x$ . Typically we detect a wide power excesses at around  $1/2f_x$ . The structures observed in subharmonic frequency range are as complex, and even more diverse, than the just described structures at  $f_x$  and its vicinity (parent frequency range, in the following).

A selection of 12 stars which show significant power excess at subharmonic frequency range is presented in Fig. 11. There are two panels for each star. Upper panel shows vicinity of the additional mode(s),  $f_x$ . Lower panel shows vicinity of its(their) subharmonic(s) at  $1/2f_x$ . The ranges of the two panels are chosen in such a way, that subharmonic of each frequency in the upper panel is located exactly underneath in the bottom panel.

Signals at subharmonic frequency range show more diverse structures than detected at the parent frequency range. We find wide bands of power excess. Again, it is difficult to select one peak to characterize a band. Typically, a signal at subharmonic frequency range fits well to a cluster of peaks detected at the parent frequency range. Examples are OGLE-BLG-RRLYR-08826, OGLE-BLG-RRLYR-07448 in Fig. 11. In general, bands of power at subharmonic frequency range are wider than clusters of peaks detected at a parent frequency range, while amplitudes of the highest peaks are often comparable or even higher at the subharmonic range.

Very interesting stars are OGLE-BLG-RRLYR-08597, -06617, -10037, -05071. In these stars there are clusters of peaks at  $f_x$  and  $1/2f_x$ , but the bands of power at subharmonic frequency range seems to be split into two subbands centered at  $\sim 1/2f_x$ . Exactly at  $1/2f_x$  the signal is suppressed. In several stars the bands of power excess are very wide. Examples of such stars in Fig. 11 are: OGLE-BLG-RRLYR-31736, -06461, -07486.

Other interesting stars are those that simultaneously show significant signals at frequencies corresponding to the three sequences, 0.61, 0.62 and 0.63. Not all of these signals have counterparts in the subharmonic frequency range. OGLE-BLG-RRLYR-08826 presented in Fig. 11 is a good example. In this star there are three clusters of peaks from the three sequences, but only a subharmonic of  $\sim 0.63$  cluster is present. OGLE-BLG-RRLYR-06610 is another good example illustrated in Fig. 11.

In a frequency spectrum of OGLE-BLG-RRLYR-05296 the dominant signal corresponds to 0.62 sequence. However, in the subharmonic frequency range a significant signal appears at frequency expected for the 0.63 sequence. Similar situation is visible in OGLE-BLG-RRLYR-08460. In the parent frequency range of this star we detect peaks corresponding to  $\sim 0.63$  sequence, but in the subharmonic fre-

quency range a signal appears at frequency expected for the  $\sim 0.61$  sequence. This may be a consequence of strong time dependence of the observed phenomena, already discussed in the previous Section.

### 3.4 Blazhko effect

In spectra of some stars from the input sample (485 stars) we detected equidistant triplets and doublets at the frequency of the first overtone and its harmonics. These are signatures of the Blazhko effect (Szabó 2014). Such stars constitute  $\approx 10$  per cent of the sample. Precise statistics and analysis of the Blazhko effect in the Galactic bulge RRc stars will be a subject of a forthcoming publication. We examined these stars for the presence of the additional mode and found it in two of them (‘bl’ in the remarks column of Tab. A1). We note that irregular phase (and also amplitude) changes are frequent in RRc stars. This non-stationarity is manifested in the frequency spectrum as a residual signal remaining close to first overtone frequency after prewhitening. This signal is either unresolved from the first overtone frequency, or only marginally resolved. All those stars are marked with ‘a’ in the remarks column of Tab. A1.

The first star showing simultaneously the additional non-radial mode and the Blazhko effect is OGLE-BLG-RRLYR-08177. Full light curve solution for this star is provided in Tab. A2. The additional non-radial mode, detected with  $S/N = 5.4$ , fits the 0.61 sequence in the Petersen diagram, as  $P_x/P_{1O} = 0.614$ . Blazhko effect is obvious in this star. Modulation is visible even in the raw data which we display in Fig. 12. In the frequency spectrum equidistant triplets are well visible; separation between triplet components corresponds to modulation period  $45.394 \pm 0.003$  days. At second harmonic a quintuplet is detected. A signal at modulation frequency,  $f_{BL}$ , is also detected in the spectrum.

The second star with additional non-radial mode and Blazhko effect is OGLE-BLG-RRLYR-32252. Full light curve solution for this star is provided in Tab. A3. In this case, the Blazhko modulation has much longer period:  $494.3 \pm 2.6$  days. As length of the OGLE-IV data is about 1336 days, the triplet components are resolved, but weakly. Unfortunately, there is no OGLE-III data for this star. In the frequency spectrum triplets are detected at  $f_{1O}$ ,  $3f_{1O}$ , and at  $4f_{1O}$  only higher frequency side-peak is detected. The star shows the additional non-radial mode that fits the 0.63 sequence. Frequency combination,  $f_x + f_{1O}$ , is detected in the spectrum as well.

### 3.5 Comparison with other studies

The subject of this paper, stars with additional non-radial mode with  $P_x/P_{1O} \approx 0.61$ , were also detected in other stellar populations, not only in the Galactic bulge. All known stars with additional non-radial mode are plotted in the Petersen diagram in Fig. 13. In this Section we compare our results with two studies. First is a study of Moskalik et al. (2015) who analysed *Kepler* observations of four RRc stars in the Cygnus field and summarized ground and space observations of other known 0.61 stars. As mentioned in the Introduction, 13 out of 14 RRc/RRd stars observed from space show the additional mode (see also footnote 2 on page

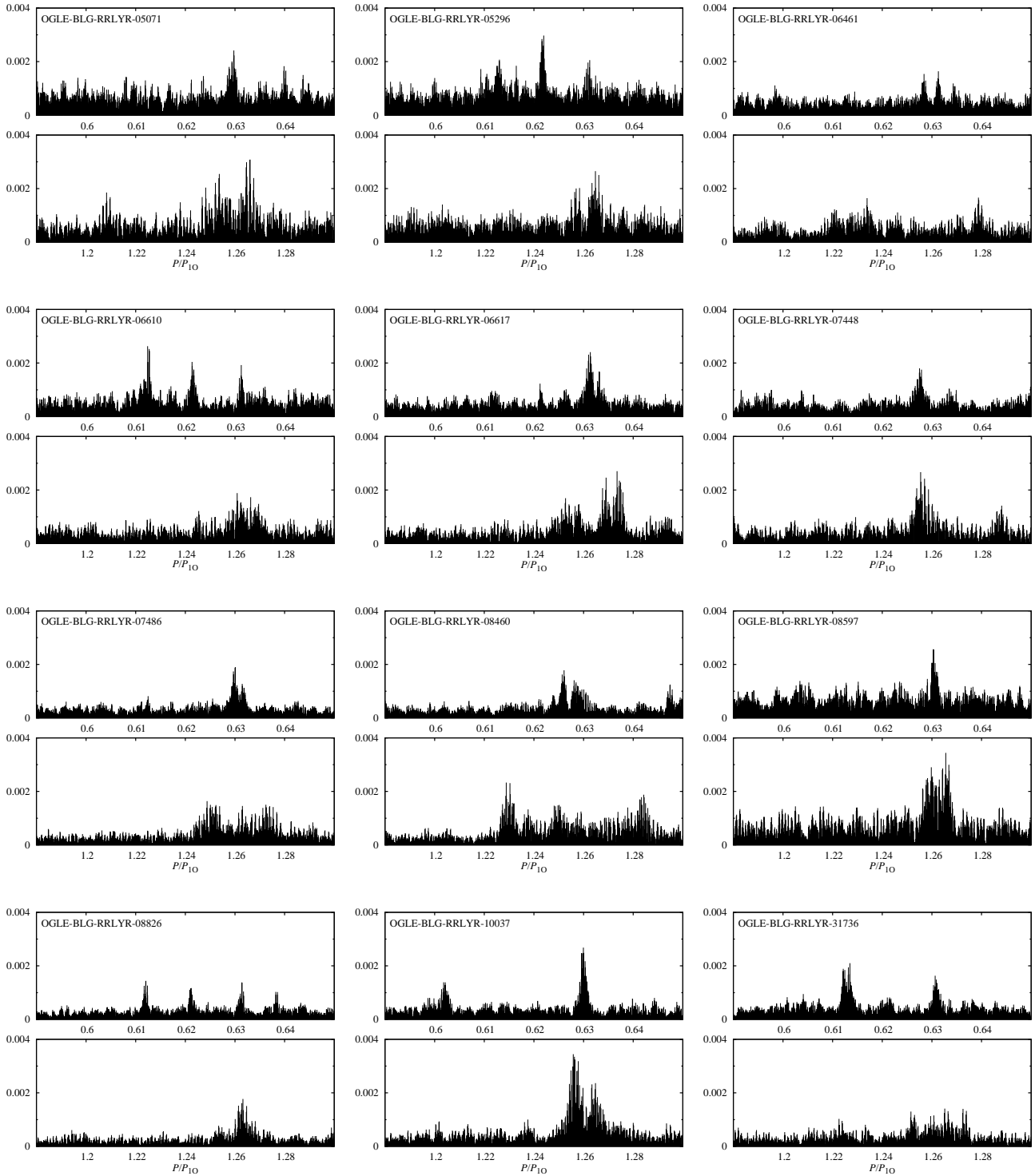


**Figure 11.** Frequency spectra centered at frequency range characteristic for additional mode (top panels) and its  $1/2$  subharmonic (bottom panels) for a sample of 0.61 stars. Horizontal axis scale is chosen such, that directly underneath a signal with frequency  $f$  (top panel) is located its subharmonic with frequency  $1/2f$  (the bottom panel).

1). In the second study, Jurcsik et al. (2015) studied the first overtone and double-mode RR Lyr stars in the globular cluster M3. In M3 the additional mode of interest was detected in 14 RRc stars (out of 37 identified as RRc) and in 4 RRd stars (out of 10); the fraction of stars showing the additional

mode in M3 is thus 38 per cent for RRc and 40 per cent for RRd stars. In our study 27 per cent of RRc stars shows the additional mode (analysed sample of 4 RRd stars, of which none shows the additional mode, is too small to draw any conclusions).

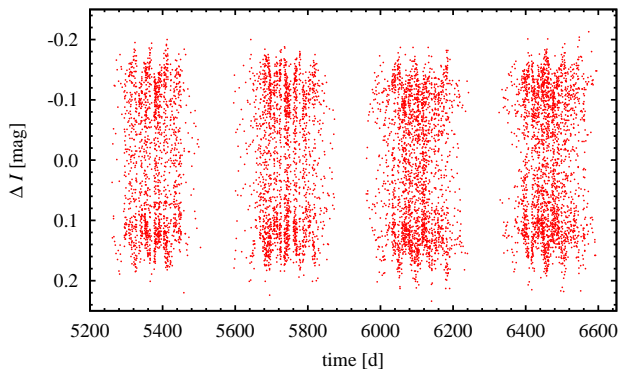


**Figure 12.** Light curve for OGLE-BLG-RRLYR-08177. Blazhko effect is clearly visible.

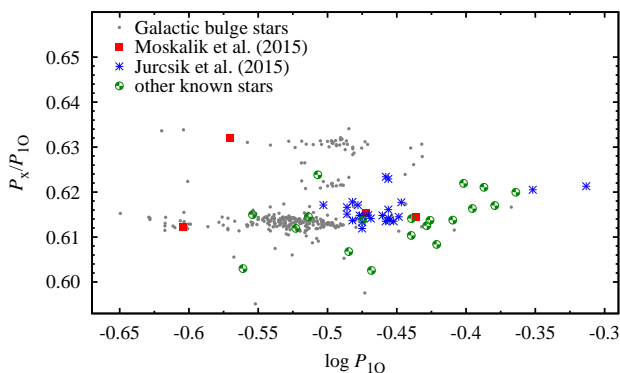


**Figure 13.** Petersen diagram for all known 0.61 stars. The Galactic bulge sample is plotted with gray dots. *Kepler* stars (Moskalik et al. 2015) and M3 stars (Jurcsik et al. 2015) are plotted with red and blue symbols, respectively. Green symbols are used for other known 0.61 stars (data from tab. 8 of Moskalik et al. 2015, see references therein).

In three stars observed by *Kepler* period ratios of additional mode to first overtone are 0.612, 0.614 and 0.616. Hence, these stars well fit the 0.61 sequence on the Petersen diagram (Fig. 13). One star has period ratio 0.632 and fits the 0.63 sequence. Most of the stars from M3 have period ratios placing them in the 0.61 sequence and in four stars period ratios correspond to 0.62 sequence. Thus, the three sequences revealed in the observations of the Galactic bulge stars seem to be present in stars from other populations as well. Very interesting result of the present study is that in single star three or two additional modes, each corresponding to one of the three sequences, may be visible simultaneously. This phenomenon is present in one star from M3, which shows two additional modes, of the 0.61 and 0.62 sequences. We also note that population effect is clearly visible in Fig. 13, when comparing the two most homogeneous samples, the Galactic bulge and M3 samples. The M3 sample covers a different period range than the Galactic bulge sample. It is also clear that the lowest sequence has, on average, a slightly larger period ratio in the M3 sample. All other stars are scattered over the diagram. Population effect is clear, but what causes the differences remains unknown. Metallicity is a first guess. We know that metallicity is an important factor influencing the period ratios of the pulsation

modes. Surprisingly, the stars from M3, where the metallicity is homogeneous (Clementini et al. 2004), show larger scatter in the Petersen diagram, than the Galactic bulge sample, where the metallicity spread is significant (Smolec 2005). What causes the difference between the properties of M3 and Galactic bulge populations remains unclear.

We note that additional non-radial modes, with characteristic period ratio,  $P_x/P_{10} \in (0.61, 0.64)$ , are also detected in classical Cepheids in both Magellanic Clouds and in one star in the Galactic disc (Moskalik & Kołaczowski 2009; Soszyński et al. 2008, 2010; Pietrukowicz et al. 2013). In the Petersen diagram (see fig. 2 in Moskalik 2014), these stars also form three nearly parallel and well separated sequences, with clear trend of decreasing period ratio with increasing period. All sequences are well populated, with largest number of stars in the lowest sequence. In the case of RR Lyr stars, majority of stars fall into the lowest sequence and spacing between sequences in the Petersen diagram is smaller.

Amplitude of the additional mode is always much lower than the amplitude of the first overtone. In stars of the Galactic bulge the amplitude ratio ranges from 0.6 to 5.5 per cent, in *Kepler* stars it is in a range of 2 to 5 per cent, and in M3 stars in a range of 2 to 8 per cent.

Properties of additional mode seem very similar in all known stars, especially its non-stationarity is visible in most of them. Variations of amplitudes and phases are very irregular and could be studied best with nearly continuous *Kepler* data. Time-dependent Fourier analysis reported in Moskalik et al. (2015) shows, that time scale of the variability ranges from 10 d to 200 d. As a result of this variability, in the frequency spectra of these stars we do not detect a single, coherent secondary peak, but either a broadened peak, or a multiplet of approximately equally spaced broadened peaks (see figs. 8 and 12 in Moskalik et al. 2015). Similar structures are also present in the frequency spectra of stars from the Galactic bulge (see Fig. 3 for some examples). In particular, in the frequency spectra of several stars from our sample, at the frequency of additional mode, we detect triplets and doublets. If these structures result from quasi-periodic modulation of additional mode, as in case of *Kepler* stars, we can estimate the time scales of this modulation from separation of the peaks. It ranges from  $\approx 20$  d to  $\approx 120$  d, with typical values corresponding to 40 – 60 d.

In all four stars observed by *Kepler*, significant signals at subharmonics of the additional mode, both at  $1/2f_x$  (in 3 stars) and at  $3/2f_x$  (in 4 stars) were detected. In OGLE-III photometry we found subharmonics at  $1/2f_x$  in four stars only. Much better OGLE-IV data allowed to find subharmonic frequency in 20 per cent of 0.61 stars, interestingly, nearly exclusively at around  $1/2f_x$ . As discussed in Sect. 3.3 and well visible in Fig. 11 signals at  $1/2f_x$  have complex structure and appear as wide bands of power excess rather than sharp peaks exactly at  $1/2f_x$ . It is also the case for *Kepler* stars. The structure of sub-harmonics at  $3/2f_x$  is plotted in fig. 8 of Moskalik et al. (2015). In Fig. 14 we plot the frequency spectra centered at  $1/2f_x$  for the three *Kepler* stars that show power excess here. Only in KIC5520878 a relatively sharp peak, centered at  $1/2f_x$  is present. For two other stars very broad bands of power excess at the vicinity of  $1/2f_x$  frequency are present, with several resolved peaks of about the same height. These structures are similar to that

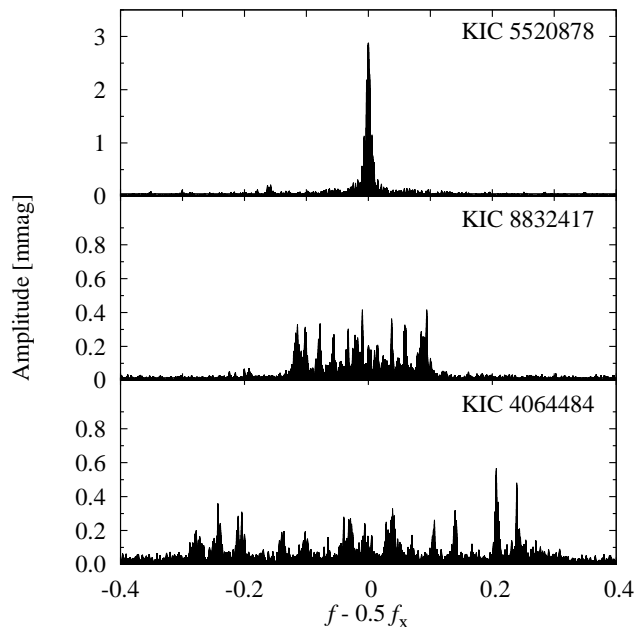


**Figure 14.** Frequency spectra of *Kepler* stars centered at subharmonic frequency  $0.5f_x$ .

observed in the Galactic bulge stars (Fig. 11). Interestingly, amplitude of highest peak at around  $1/2f_x$  in the Galactic bulge stars might be higher than amplitudes of the additional mode. Examples include OGLE-BLG-RRLYR-08597, -10037, -05071, -08460, -07448 in Fig. 11. Subharmonics were not detected in M3 stars.

#### 4 SUMMARY AND CONCLUSIONS

We analyzed OGLE-IV photometry of the first overtone and double-mode RR Lyrae stars (RRc and RRd stars, respectively) of the Galactic bulge. We limited the scope of the study to two fields with highest cadence, for which more than 8000 measurements have been accumulated over 4 years. Our sample consists of 485 RRc stars and 4 RRd stars. The main goal of this project was to search for secondary non-radial modes with period ratio to the first radial overtone of  $P_x/P_{1O} \sim 0.61$ .

The most important results of our study can be summarized as follows.

- Low amplitude secondary modes,  $f_x$ , with period ratio of  $\sim 0.61$  are detected in 131 RRc stars. This constitutes 27 per cent of the studied sample. The inferred occurrence rate is an order of magnitude higher than determined for the Galactic bulge with the OGLE-III data (3 per cent, Netzel, Smolec & Moskalik 2015) and is comparable to that found in the globular cluster M3 (38 per cent, Jurcsik et al. 2015). No additional modes beyond the radial ones are detected in the 4 RRd stars of our sample.

- The amplitudes of the secondary modes are very low, in the mmag range and do not exceed 5.5 per cent of the amplitude of the dominant first radial overtone. This upper limit is somewhat lower, but similar to that found in other studies (e.g. Olech & Moskalik 2009; Moskalik et al.

2015; Netzel, Smolec & Moskalik 2015; Jurcsik et al. 2015; Molnár et al. 2015).

- We detect the secondary modes in two stars displaying a long-term modulation of the radial mode (Blazhko effect). Three similar variables have also been found recently in M3 (Jurcsik et al. 2015). Thus, excitation of non-radial mode with  $P_x/P_{1O} \sim 0.61$  and the Blazhko modulation of the radial mode are not mutually exclusive.

- Combining the results of this paper with those of our previous analysis of OGLE-III data (Netzel, Smolec & Moskalik 2015), we now know 262 Galactic bulge RR Lyrae stars (260 RRc and 2 RRd), in which non-radial modes with period ratio of  $\sim 0.61$  are excited. This is by far the largest homogeneous sample of this type of objects.

- The period ratios measured in Galactic bulge RRc/RRd stars are all in a narrow range of  $P_x/P_{1O} = 0.598 - 0.634$ . When plotted on the period ratio vs. period diagram (so-called Petersen diagram), these stars form three, approximately parallel sequences. The sequences are nearly horizontal and are centered at  $P_x/P_{1O} \approx 0.613$ ,  $\approx 0.623$  and  $\approx 0.631$ . The lowest sequence is by far most populated. The sequence at  $\approx 0.631$  was tentatively identified by Netzel, Smolec & Moskalik (2015) and is now fully confirmed. The middle sequence at  $\approx 0.623$  is identified for the first time.

- The existence of the three sequences of RRc stars is analogous to behaviour of the first overtone Cepheids. In the later case, non-radial modes with  $P_x/P_{1O} = 0.60 - 0.65$  have been detected in more than 170 objects. These Cepheids form three parallel sequences in the Petersen diagram as well (for summary see Moskalik 2014).

- In 20 OGLE-IV RRc stars we detected more than one secondary mode. In 14 variables two secondary modes belonging to two different sequences are present. In 6 variables three secondary modes representing all three sequences are present. Clearly, modes of different sequences can be excited simultaneously in the same star.

- Secondary modes are in many cases non-stationary, changing their amplitude and frequency from season to season and during the seasons. Consequently, in the Fourier transform of entire dataset, they do not appear as single, coherent peaks, but rather as broadened peaks or as narrow bands of power (clusters of peaks).

- In 7 OGLE-IV RRc stars a secondary mode is split into three almost equally spaced clusters of peaks. In further 10 stars a secondary mode is split into two components. As was shown in case of *Kepler* RRc stars, such structure might result from quasi-periodic modulation of the mode (Moskalik et al. 2015, see their Fig. 12). The splittings observed in OGLE-IV RRc stars correspond to modulation timescales of 20 – 120 d. Both non-stationarity and splitting occur most frequently for modes of sequence 0.61.

- In 26 OGLE-IV RRc stars a significant signal at around  $\sim 1/2f_x$ , i.e. at around a subharmonic of the secondary frequency is found. This constitutes 20 per cent of all 0.61 stars identified in this study. A subharmonic at around  $\sim 3/2f_x$  is found in two stars. Until now, subharmonics of  $f_x$  have been detected only in RRc and RRd variables observed from space. With the OGLE data, we have for the first time a possibility to see them from the ground (see also Netzel et al. 2015). Judging from space photometry, subharmon-

ics are common and occur in at least 75 per cent of the 0.61 variables (Moskalik et al. 2015). Their presence is a signature of a period doubling of the secondary oscillation (e.g. Smolec et al. 2012).

- Subharmonic signal is highly non-coherent. We always detect a band of power, located at around the subharmonic frequency,  $1/2f_x$ . This band of power is usually broader and sometimes much broader than the cluster of peaks corresponding to the parent mode,  $f_x$ . In addition, it often displays a wide, essentially flat structure or a bimodal structure, not seen in the parent mode. When more than one secondary mode is present, subharmonics structures often are seen only for one of them, and this is not always the one with the largest amplitude. We note, that similar broad bands of power at  $1/2f_x$  are also detected in two RRc stars studied by *Kepler* space telescope (Moskalik et al. 2015, and our Fig. 14). Clearly, the subharmonics of the secondary modes are non-stationary to even larger degree than the modes themselves.

The discussed stars with additional non-radial mode are not well understood. We do not know which non-radial mode is excited and what is the mechanism behind its excitation. The only and unsuccessful attempt to understand these stars is a work by Dziembowski (2012) focused on classical Cepheids. Recently, Lindner et al. (2015) noticed that period ratio in the discussed stars is close to the reciprocal of the golden ratio, which is  $\approx 0.618033$ , and argued that pulsation with such a period ratio of the excited modes should be stable against perturbations. They refer to 0.61 stars as *golden stars*. A glimpse at the Petersen diagram (Fig. 13) shows, that such explanation is unlikely. The stars are indeed located close to the reciprocal of the golden ratio, but do not cluster at it. The reciprocal of the golden ratio falls in between the lowest and the middle sequences and clearly *does not attract* any of the stars. The proximity of the period ratio in 0.61 stars to the reciprocal of the golden ratio is a pure coincidence in our opinion, and explanation for the stars, on solid grounds of pulsation theory, must be searched for.

## ACKNOWLEDGEMENTS

This research is supported by the Polish National Science Centre through grant DEC-2012/05/B/ST9/03932.

We are grateful to the referee, Johanna Jurcsik, for constructive comments, which helped to improve this publication.

## REFERENCES

- Alcock C., Alves D.R., Becker Al. et al., 2003, ApJ, 598, 597
- Clementini G., Corwin. T.M., Carney B.W., Smerel A.N., 2004, ApJ, 127, 938
- Dziembowski W., 2012, Acta Astron., 62, 323
- Gruberbauer M., Kolenberg K., Rowe J. et al., 2007, MNRAS, 379, 1498
- Jurcsik J., et al., 2009, MNRAS, 400, 1006
- Jurcsik J., Smitola P., Hajdu G., Nuspl J., 2014, ApJ, 797, L3
- Jurcsik J., et al., 2015, ApJ Suppl. Ser., in press, arXiv:1504.06215
- Kolenberg K., et al., 2010, ApJ, 713, L198
- Lindner J.F., Kohar V., Kia B., Hippke M., Learned J.G., Ditto, W.L., 2015, Phys. Rev. Lett., 114, 054101
- Molnár L., et al. 2015, MNRAS, submitted
- Moskalik P., 2013, in Suárez J.C., Garrido R., Balona L.A., Christensen-Dalsgaard J., eds, Astrophysics and Space Sci. Proc. 31, Stellar Pulsations: Impact of New Instrumentation and New Insights. Springer-Verlag, Berlin, Heidelberg, p. 103
- Moskalik P., 2014, in Guzik J.A., Chaplin W.J., Handler G., Pigulski A., eds, IAU Symp. 301, p. 249
- Moskalik P., Kołaczkowski Z., 2009, MNRAS, 394, 1649
- Moskalik P., et al., 2013, in Suárez J.C., Garrido R., Balona L.A., Christensen-Dalsgaard J., eds, Astrophysics and Space Sci. Proc. 31, Stellar Pulsations: Impact of New Instrumentation and New Insights. Springer-Verlag, Berlin, Heidelberg, poster no. 34; Online data at [http://dx.doi.org/10.1007/978-3-642-29630-7\\_53](http://dx.doi.org/10.1007/978-3-642-29630-7_53)
- Moskalik P., Smolec R., Kolenberg K. et al., 2015, MNRAS, 447, 2348
- Netzel H., Smolec R., Moskalik P., 2015, MNRAS, 447, 1173
- Netzel H., Smolec R., Dziembowski W., 2015, MNRAS Lett., 451, L25
- Olech A., Moskalik P., 2009, A&A, 494, L17
- Pietrukowicz P., et al., 2013, Acta Astron., 63, 379
- Smolec R., 2005, Acta Astron., 55, 59
- Smolec R., Soszyński I., Moskalik P., et al., 2012, MNRAS, 419, 2407
- Smolec R., Soszyński I., Udalski A. et al., 2015, MNRAS, 447, 3756
- Soszyński I., Poleski R., Udalski A., et al., 2008, Acta Astron., 58, 163
- Soszyński I., Udalski A., Szymański M.K. et al., 2009, Acta Astron., 59, 1
- Soszyński I., Poleski R., Udalski A., et al., 2010, Acta Astron., 60, 17
- Soszyński I., Dziembowski W., Udalski A., et al., 2011, Acta Astron., 61, 1
- Soszyński I., Udalski A., Szymański M.K. et al., 2014, Acta Astron., 64, 177
- Szabó R., 2014, IAUS, 301, 241
- Szabó R., Kolláth Z., Molnár L. et al., 2010, MNRAS, 409, 1244
- Szabó R., Benkó J.M., Paparó M., 2014, A&A, 570, A100
- Süveges M., Sesar B., Váradi M. et al., 2012, MNRAS, 424, 2528
- Udalski A., Szymański M.K., Soszyński I., Poleski R., 2008, Acta Astron., 58, 69
- Udalski A., Szymański M.K., Szymański G., 2015, Acta Astron., 65, 1

**APPENDIX A: LIST OF 0.61 STARS**

This paper has been typeset from a  $\text{\TeX}$ / $\text{\LaTeX}$  file prepared by the author.

**Table A1.** Properties of stars with non-radial mode (OGLE-IV)

a - period change; bl - Blazhko effect; td - signal visible only after time-dependent prewhitening;  
c - combination frequency; s - power excess at subharmonic; d - doublet; t - triplet; e - additional frequency;  
g - non-stationary  $f_x$ ; f - complex structure of  $f_x$ ; sr - half of the first season removed  
h - stars detected in OGLE-III data (Netzel, Smolec & Moskalik 2015)

Name	$P_{1O}$ [d]	$P_x$ [d]	$P_x/P_{1O}$	$A_{1O}$ [mag]	$A_x$ [mag]	$A_x/A_{1O}$	Remarks
OGLE-BLG-RRLYR-04067	0.31994	0.19592	0.61236	0.10687	0.00479	0.0448	a
OGLE-BLG-RRLYR-04105	0.30582	0.18724	0.61226	0.13009	0.00476	0.0366	
OGLE-BLG-RRLYR-04549	0.29964	0.18874	0.62990	0.12246	0.00384	0.0313	
OGLE-BLG-RRLYR-04599	0.28939	0.17797	0.61498	0.13980	0.00340	0.0243	a,g
OGLE-BLG-RRLYR-04754	0.28631	0.17578	0.61394	0.12788	0.00453	0.0354	g,h
OGLE-BLG-RRLYR-04762	0.29465	0.18061	0.61295	0.12640	0.00700	0.0554	
OGLE-BLG-RRLYR-04902	0.32219	0.19728	0.61230	0.12395	0.00314	0.0253	g
OGLE-BLG-RRLYR-04942	0.31855	0.19534	0.61320	0.09610	0.00305	0.0317	sr
OGLE-BLG-RRLYR-04974	0.29665	0.18163	0.61228	0.12452	0.00436	0.0350	t
OGLE-BLG-RRLYR-04989	0.30670	0.18767	0.61191	0.13024	0.00247	0.0190	a,g
OGLE-BLG-RRLYR-05071	0.33469	0.21078	0.62978	0.13613	0.00255	0.0187	a,s
OGLE-BLG-RRLYR-05141	0.29274	0.17963	0.61362	0.12807	0.00434	0.0339	
OGLE-BLG-RRLYR-05201	0.29693	0.18220	0.61361	0.12856	0.00453	0.0353	a,g
OGLE-BLG-RRLYR-05231	0.28601	0.17575	0.61450	0.14483	0.00178	0.0123	a,g
OGLE-BLG-RRLYR-05266	0.30485	0.18925	0.62079	0.12610	0.00294	0.0233	a,g
	0.30485	0.18670	0.61244	0.12610	0.00217	0.0172	
OGLE-BLG-RRLYR-05291	0.32072	0.19692	0.61398	0.11398	0.00229	0.0201	a,c
OGLE-BLG-RRLYR-05296	0.31873	0.19823	0.62195	0.13114	0.00291	0.0222	c,g,s
OGLE-BLG-RRLYR-05301	0.30562	0.18729	0.61282	0.12450	0.00554	0.0445	a,c,g,h
OGLE-BLG-RRLYR-05527	0.28715	0.17593	0.61266	0.12418	0.00230	0.0185	c,f
OGLE-BLG-RRLYR-05531	0.30808	0.18908	0.61372	0.09446	0.00304	0.0322	g
OGLE-BLG-RRLYR-05542	0.28751	0.17730	0.61668	0.14280	0.00154	0.0108	a,f
OGLE-BLG-RRLYR-05600	0.30881	0.18947	0.61355	0.13017	0.00340	0.0261	c,t
OGLE-BLG-RRLYR-05672	0.28435	0.17464	0.61420	0.14864	0.00170	0.0114	g
OGLE-BLG-RRLYR-05898	0.32687	0.20613	0.63060	0.13245	0.00361	0.0272	a
OGLE-BLG-RRLYR-05924	0.29997	0.18412	0.61380	0.14345	0.00447	0.0312	a,c
OGLE-BLG-RRLYR-05928	0.31043	0.19071	0.61434	0.10101	0.00129	0.0128	a
OGLE-BLG-RRLYR-05934	0.29263	0.17948	0.61334	0.13069	0.00279	0.0214	a,g
OGLE-BLG-RRLYR-05937	0.31421	0.19241	0.61235	0.12346	0.00370	0.0300	a,g
OGLE-BLG-RRLYR-05965	0.31396	0.19266	0.61364	0.11521	0.00308	0.0267	a,g
OGLE-BLG-RRLYR-06056	0.33646	0.20105	0.59756	0.15306	0.00179	0.0117	a
OGLE-BLG-RRLYR-06083	0.30647	0.18756	0.61199	0.13596	0.00338	0.0249	f
OGLE-BLG-RRLYR-06130	0.30384	0.18632	0.61323	0.09404	0.00222	0.0237	d,e
OGLE-BLG-RRLYR-06143	0.30875	0.18947	0.61368	0.12086	0.00282	0.0233	c,g
OGLE-BLG-RRLYR-06149	0.27854	0.17084	0.61334	0.10532	0.00194	0.0184	d
OGLE-BLG-RRLYR-06194	0.30451	0.19077	0.62650	0.11891	0.00168	0.0141	a
OGLE-BLG-RRLYR-06200	0.28699	0.17647	0.61490	0.14828	0.00306	0.0206	a,c,t
OGLE-BLG-RRLYR-06265	0.32974	0.20719	0.62833	0.12563	0.00223	0.0178	a
OGLE-BLG-RRLYR-06420	0.31401	0.19246	0.61290	0.10435	0.00348	0.0333	a,c,h
	0.31401	0.19542	0.62233	0.10435	0.00188	0.0181	
OGLE-BLG-RRLYR-06461	0.29651	0.18719	0.63130	0.13055	0.00186	0.0142	
OGLE-BLG-RRLYR-06497	0.28119	0.17230	0.61276	0.15406	0.00524	0.0340	c,e,t
OGLE-BLG-RRLYR-06571	0.29408	0.18155	0.61734	0.11915	0.00147	0.0124	a
OGLE-BLG-RRLYR-06590	0.33661	0.21246	0.63118	0.13126	0.00228	0.0174	a,e
OGLE-BLG-RRLYR-06610	0.31623	0.19649	0.62135	0.11623	0.00196	0.0169	a,s
	0.31623	0.19377	0.61274	0.11623	0.00245	0.0211	
	0.31623	0.19963	0.63126	0.11623	0.00188	0.0162	
OGLE-BLG-RRLYR-06617	0.32632	0.20603	0.63137	0.13774	0.00251	0.0182	a,g
OGLE-BLG-RRLYR-06627	0.29820	0.18072	0.60602	0.11553	0.00202	0.0175	a,c,d,g
OGLE-BLG-RRLYR-06659	0.28984	0.17607	0.60746	0.11661	0.00222	0.0191	a,c,d,g
OGLE-BLG-RRLYR-06693	0.29235	0.17935	0.61349	0.14231	0.00360	0.0253	a,g
OGLE-BLG-RRLYR-06802	0.31830	0.19501	0.61267	0.11096	0.00213	0.0192	a,c,g,s,td
	0.31830	0.19792	0.62181	0.11096	0.00207	0.0186	
	0.31830	0.20098	0.63142	0.11096	0.00169	0.0152	
OGLE-BLG-RRLYR-06885	0.28525	0.17527	0.61445	0.15038	0.00227	0.0151	a,g
OGLE-BLG-RRLYR-07076	0.29638	0.18209	0.61437	0.12542	0.00202	0.0161	a,t,h

Name	$P_{1O}$ [d]	$P_x$ [d]	$P_x/P_{1O}$	$A_{1O}$ [mag]	$A_x$ [mag]	$A_x/A_{1O}$	Remarks
OGLE-BLG-RRLYR-07091	0.27903	0.17095	0.61266	0.14490	0.00216	0.0149	a,t
OGLE-BLG-RRLYR-07094	0.26797	0.16458	0.61418	0.10938	0.00210	0.0192	a,g,h
OGLE-BLG-RRLYR-07096	0.31880	0.19548	0.61317	0.11715	0.00263	0.0225	a,c,d,g
OGLE-BLG-RRLYR-07103	0.30453	0.18608	0.61102	0.12448	0.00305	0.0245	
OGLE-BLG-RRLYR-07135	0.35978	0.22448	0.62392	0.10472	0.00138	0.0132	a,s
OGLE-BLG-RRLYR-07292	0.32493	0.20495	0.63075	0.13019	0.00235	0.0181	a,g,s
OGLE-BLG-RRLYR-07303	0.32197	0.20048	0.62267	0.12339	0.00193	0.0157	a,c
OGLE-BLG-RRLYR-07375	0.32464	0.20176	0.62148	0.12227	0.00266	0.0218	a,c,s
	0.32464	0.19891	0.61270	0.12227	0.00139	0.0114	
OGLE-BLG-RRLYR-07448	0.37014	0.23241	0.62788	0.07002	0.00177	0.0252	s
OGLE-BLG-RRLYR-07486	0.31703	0.19974	0.63005	0.14016	0.00218	0.0156	a,c,g,s
OGLE-BLG-RRLYR-07500	0.32308	0.20407	0.63163	0.12655	0.00111	0.0087	a,s,c,e
	0.32308	0.20081	0.62157	0.12655	0.00128	0.0101	
OGLE-BLG-RRLYR-07517	0.32565	0.20497	0.62943	0.12239	0.00236	0.0193	a,g,s
OGLE-BLG-RRLYR-07518	0.29361	0.18029	0.61405	0.13590	0.00373	0.0275	a,c,g,h
OGLE-BLG-RRLYR-07559	0.32052	0.19617	0.61204	0.11084	0.00152	0.0137	a,c,g,s
	0.32052	0.20239	0.63144	0.11086	0.00124	0.0112	
OGLE-BLG-RRLYR-07677	0.29486	0.18080	0.61318	0.11823	0.00341	0.0288	g
OGLE-BLG-RRLYR-07701	0.29796	0.18267	0.61309	0.14771	0.00227	0.0154	a,g
OGLE-BLG-RRLYR-07714	0.36978	0.22641	0.61227	0.12508	0.00132	0.0106	a,c,g
OGLE-BLG-RRLYR-07723	0.35599	0.21762	0.61131	0.13238	0.00175	0.0132	a,s
OGLE-BLG-RRLYR-07781	0.42917	0.26464	0.61664	0.12329	0.00194	0.0157	a,td,c
OGLE-BLG-RRLYR-07803	0.31390	0.19220	0.61230	0.12436	0.00285	0.0229	a,c,g
OGLE-BLG-RRLYR-07806	0.31900	0.19820	0.62131	0.12226	0.00190	0.0156	a,c,s,g
	0.31900	0.19547	0.61276	0.12226	0.00168	0.0138	
	0.31900	0.20132	0.63109	0.12226	0.00149	0.0122	
OGLE-BLG-RRLYR-07857	0.32088	0.19645	0.61224	0.12395	0.00156	0.0126	a,c,s
	0.32088	0.19938	0.62137	0.12395	0.00222	0.0179	
OGLE-BLG-RRLYR-07907	0.28779	0.17659	0.61360	0.14599	0.00398	0.0273	
OGLE-BLG-RRLYR-07962	0.24463	0.14982	0.61244	0.11238	0.00311	0.0277	c,d
OGLE-BLG-RRLYR-08002	0.30879	0.18918	0.61264	0.11784	0.00267	0.0227	a,c,f,g
	0.30879	0.19471	0.63055	0.11784	0.00152	0.0129	
OGLE-BLG-RRLYR-08123	0.28762	0.18132	0.63042	0.12587	0.00150	0.0119	a
	0.28762	0.17583	0.61134	0.12587	0.00199	0.0158	
OGLE-BLG-RRLYR-08125	0.27681	0.16954	0.61246	0.10073	0.00453	0.0450	a,c,e,g,h
	0.27681	0.17468	0.63103	0.10073	0.00188	0.0187	
OGLE-BLG-RRLYR-08137	0.30800	0.18914	0.61411	0.12859	0.00296	0.0231	a,c,g
OGLE-BLG-RRLYR-08138	0.31864	0.19525	0.61276	0.12119	0.00131	0.0108	a,e,s,td
	0.31864	0.20104	0.63093	0.12119	0.00143	0.0118	
OGLE-BLG-RRLYR-08170	0.32306	0.19797	0.61281	0.11671	0.00151	0.0130	a,g
OGLE-BLG-RRLYR-08177	0.28513	0.17518	0.61438	0.14088	0.00204	0.0145	bl
OGLE-BLG-RRLYR-08302	0.29946	0.18393	0.61421	0.13206	0.00273	0.0207	a,g
OGLE-BLG-RRLYR-08390	0.29069	0.17800	0.61233	0.13221	0.00192	0.0145	a,c
OGLE-BLG-RRLYR-08421	0.30188	0.18461	0.61153	0.12594	0.00330	0.0262	a,g,h
OGLE-BLG-RRLYR-08447	0.27066	0.16390	0.60555	0.15470	0.00106	0.0069	
OGLE-BLG-RRLYR-08460	0.36490	0.22846	0.62609	0.11244	0.00177	0.0157	a,c,d,s
OGLE-BLG-RRLYR-08590	0.24166	0.14847	0.61438	0.08419	0.00267	0.0317	a,g
OGLE-BLG-RRLYR-08594	0.29979	0.18356	0.61231	0.13151	0.00519	0.0395	a,c,g
OGLE-BLG-RRLYR-08597	0.32093	0.20228	0.63031	0.13666	0.00279	0.0204	a,s,h
OGLE-BLG-RRLYR-08653	0.36015	0.22232	0.61731	0.13333	0.00131	0.0098	a
OGLE-BLG-RRLYR-08674	0.31692	0.19433	0.61319	0.12192	0.00186	0.0152	a,c,g,s,h
OGLE-BLG-RRLYR-08696	0.32765	0.20421	0.62326	0.12791	0.00125	0.0098	a,td,c,g,s
	0.32765	0.20775	0.63407	0.12791	0.00134	0.0104	
OGLE-BLG-RRLYR-08715	0.36986	0.23325	0.63064	0.12879	0.00173	0.0134	a
OGLE-BLG-RRLYR-08720	0.27942	0.17212	0.61598	0.15325	0.00135	0.0088	a,c,g,sr
OGLE-BLG-RRLYR-08721	0.24132	0.14756	0.61146	0.08050	0.00410	0.0510	a,c,f,h
OGLE-BLG-RRLYR-08824	0.30036	0.18370	0.61162	0.12436	0.00399	0.0321	a,c,f,g
OGLE-BLG-RRLYR-08826	0.31251	0.19127	0.61204	0.10170	0.00166	0.0163	a,c,s
	0.31251	0.19732	0.63140	0.10170	0.00149	0.0146	
	0.31251	0.19404	0.62089	0.10170	0.00100	0.0099	



Name	$P_{1O}$ [d]	$P_x$ [d]	$P_x/P_{1O}$	$A_{1O}$ [mag]	$A_x$ [mag]	$A_x/A_{1O}$	Remarks
OGLE-BLG-RRLYR-08844	0.28957	0.17753	0.61307	0.12863	0.00261	0.0203	g
OGLE-BLG-RRLYR-08847	0.26403	0.16192	0.61327	0.07226	0.00172	0.0238	g
OGLE-BLG-RRLYR-08863	0.28168	0.17291	0.61388	0.14696	0.00175	0.0119	a,s
OGLE-BLG-RRLYR-08866	0.24142	0.14800	0.61304	0.13513	0.00227	0.0168	g
OGLE-BLG-RRLYR-08986	0.30559	0.18777	0.61445	0.12067	0.00303	0.0251	
OGLE-BLG-RRLYR-09126	0.32399	0.20138	0.62156	0.12484	0.00282	0.0226	a,c,g,s
	0.32399	0.19847	0.61260	0.12484	0.00231	0.0185	
	0.32399	0.20468	0.63177	0.12484	0.00143	0.0115	
OGLE-BLG-RRLYR-09164	0.28639	0.17558	0.61309	0.14306	0.00307	0.0214	c,g,h
OGLE-BLG-RRLYR-09212	0.23495	0.14436	0.61441	0.12440	0.00178	0.0143	a,g
OGLE-BLG-RRLYR-09305	0.30295	0.18586	0.61350	0.12718	0.00428	0.0337	a,c,g,s,h
	0.30295	0.18858	0.62248	0.12718	0.00153	0.0121	
	0.30295	0.19126	0.63132	0.12718	0.00171	0.0135	
OGLE-BLG-RRLYR-09436	0.33013	0.20362	0.61678	0.12507	0.00178	0.0142	a,c,g
OGLE-BLG-RRLYR-09511	0.30283	0.18971	0.62648	0.11040	0.00161	0.0146	a
OGLE-BLG-RRLYR-09520	0.24893	0.15259	0.61300	0.10905	0.00154	0.0142	e
OGLE-BLG-RRLYR-09521	0.32318	0.19808	0.61291	0.11586	0.00133	0.0115	a,s
	0.32318	0.20428	0.63209	0.11586	0.00114	0.0098	
OGLE-BLG-RRLYR-09529	0.30693	0.18842	0.61390	0.12524	0.00383	0.0306	a,c,d,f,h
OGLE-BLG-RRLYR-09631	0.28027	0.17236	0.61498	0.14639	0.00127	0.0087	a,g
OGLE-BLG-RRLYR-09649	0.30893	0.19014	0.61547	0.11701	0.00376	0.0321	a,g
OGLE-BLG-RRLYR-09665	0.29925	0.18352	0.61325	0.11705	0.00381	0.0325	g
OGLE-BLG-RRLYR-09696	0.30839	0.18772	0.60872	0.11066	0.00069	0.0063	a,g
OGLE-BLG-RRLYR-09775	0.23541	0.14451	0.61389	0.09353	0.00174	0.0186	
OGLE-BLG-RRLYR-09795	0.31620	0.19441	0.61485	0.15930	0.00127	0.0080	a,g,c
OGLE-BLG-RRLYR-10000	0.29739	0.18269	0.61431	0.12806	0.00246	0.0192	a,d
OGLE-BLG-RRLYR-10008	0.30435	0.18729	0.61536	0.12697	0.00259	0.0204	a,f
OGLE-BLG-RRLYR-10037	0.32980	0.20776	0.62997	0.13112	0.00278	0.0212	a,c,g,s,h
OGLE-BLG-RRLYR-10040	0.31351	0.19233	0.61345	0.13149	0.00200	0.0152	a,c,d,f
OGLE-BLG-RRLYR-10127	0.28186	0.17317	0.61438	0.14131	0.00219	0.0155	a
OGLE-BLG-RRLYR-10371	0.28935	0.17718	0.61235	0.13613	0.00243	0.0178	a,c,g,e,s,h
OGLE-BLG-RRLYR-30633	0.29150	0.17891	0.61376	0.12989	0.00287	0.0221	
OGLE-BLG-RRLYR-30848	0.30693	0.18930	0.61676	0.12281	0.00234	0.0190	a,g
OGLE-BLG-RRLYR-31736	0.30524	0.18726	0.61348	0.13337	0.00207	0.0155	a,c,g,s
	0.30524	0.19250	0.63065	0.13337	0.00157	0.0118	
OGLE-BLG-RRLYR-32091	0.28894	0.17691	0.61225	0.12991	0.00353	0.0271	a,t
OGLE-BLG-RRLYR-32145	0.30005	0.18422	0.61397	0.11418	0.00340	0.0298	a,c,g
OGLE-BLG-RRLYR-32252	0.36310	0.22868	0.62980	0.11697	0.00207	0.0177	bl,c
OGLE-BLG-RRLYR-32289	0.30627	0.18845	0.61529	0.12610	0.00265	0.0210	a,c,g
OGLE-BLG-RRLYR-32877	0.25066	0.15337	0.61186	0.07322	0.00349	0.0477	
	0.25066	0.15600	0.62235	0.07322	0.00247	0.0337	

**Table A2.** Light curve solution for OGLE-BLG-RRLYR-08177.

freq. id	$f$ [d <sup>-1</sup> ]	$A$ [mag]	$\sigma$	$\phi$ [rad]	$\sigma$
$f_{\text{BL}}$	0.02202965	0.0017	0.0003	0.12	0.17
$f_{10} - f_{\text{BL}}$	3.48509951	0.0334	0.0003	3.559	0.083
$f_{10}$	3.50712916	0.1408	0.0003	2.889	0.023
$f_{10} + f_{\text{BL}}$	3.52915881	0.0256	0.0003	6.215	0.090
$f_x$	5.70840168	0.0020	0.0003	3.0	1.9
$2f_{10} - 2f_{\text{BL}}$	6.97019902	0.0017	0.0003	3.71	0.22
$2f_{10} - f_{\text{BL}}$	6.99222868	0.0127	0.0003	2.165	0.091
$2f_{10}$	7.01425833	0.0200	0.0003	2.665	0.048
$2f_{10} + f_{\text{BL}}$	7.03628798	0.0059	0.0003	5.64	0.11
$2f_{10} + 2f_{\text{BL}}$	7.05831763	0.0014	0.0003	2.83	0.26
$3f_{10} - 2f_{\text{BL}}$	10.47732819	0.0028	0.0003	1.53	0.19
$3f_{10} - f_{\text{BL}}$	10.49935784	0.0057	0.0003	1.90	0.11
$3f_{10}$	10.52138749	0.0140	0.0003	2.632	0.071
$3f_{10} + f_{\text{BL}}$	10.54341714	0.0029	0.0003	6.04	0.15
$4f_{10} - f_{\text{BL}}$	14.00648700	0.0031	0.0003	1.93	0.14
$4f_{10}$	14.02851665	0.0085	0.0003	2.676	0.096
$4f_{10} + f_{\text{BL}}$	14.05054631	0.0028	0.0003	6.11	0.16
$5f_{10} - f_{\text{BL}}$	17.51361617	0.0019	0.0003	1.77	0.19
$5f_{10}$	17.53564582	0.0050	0.0003	2.22	0.12
$5f_{10} + f_{\text{BL}}$	17.55767547	0.0023	0.0003	5.55	0.19
$6f_{10}$	21.04277498	0.0030	0.0003	1.52	0.16
$7f_{10}$	24.54990414	0.0015	0.0003	0.64	0.23

**Table A3.** Light curve solution for OGLE-BLG-RRLYR-32252.

freq. id	$f$ [d <sup>-1</sup> ]	$A$ [mag]	$\sigma$	$\phi$ [rad]	$\sigma$
$f_{10} - f_{\text{BL}}$	2.75202958	0.0073	0.0003	4.69	0.37
$f_{10}$	2.75405244	0.1169	0.0002	4.806	0.048
$f_{10} + f_{\text{BL}}$	2.75607531	0.0080	0.0003	1.61	0.43
$f_x$	4.37567732	0.0020	0.0002	0.7	1.3
$2f_{10}$	5.50810489	0.0067	0.0002	1.01	0.10
$f_{10} + f_x$	7.12972977	0.0017	0.0002	0.6	1.3
$3f_{10} - f_{\text{BL}}$	8.26013447	0.0017	0.0002	3.16	0.35
$3f_{10}$	8.26215733	0.0075	0.0002	3.50	0.15
$3f_{10} + f_{\text{BL}}$	8.26418020	0.0018	0.0002	0.16	0.51
$4f_{10}$	11.01620978	0.0043	0.0002	5.42	0.20
$4f_{10} + f_{\text{BL}}$	11.01823264	0.0012	0.0002	2.17	0.57
$5f_{10}$	13.77026222	0.0025	0.0002	0.91	0.26
$6f_{10}$	16.52431467	0.0013	0.0002	2.54	0.34